Laser Particle Acceleration

3.1 Plasmas

The plasma state is a state of matter where components are no more neutral; this is usually reached when a bulk is heated to a point where its internal energy is higher than one or more ionization levels, which makes the single atoms to lose electrons in collisions. A plasma can be locally created by ionizing a certain amount of material, like in discharge tubes, heating a rarefied gas with microwaves or by interaction with a laser. The vast set of parameters, in temperature, pressure, density, neutrality makes the plasma state one of the most various chapter of the physics.

Collective parameters In a plasma, for each of the species α, it is defined the α-plasma frequency

$$\omega_{p\alpha} = \sqrt{\frac{n_\alpha q_\alpha^2}{\varepsilon_0 m_\alpha}}, \tag{3.1}$$

which is the oscillating frequency of the α component. This is a key parameter for evaluating the response timescale of the α-plasma to external fields. When a separation of charges is produced, the motion of the α component to restore the neutrality results in an oscillation at the frequency (3.1).

For each charge in a plasma, the surrounding charge distribution balances its electrostatic potential, which effectively screens it, lowering the distance over which its influence should be considered effective. The distance over which the newly created electric field

drops by a factor of $1/e$ is the Debye length[13]:

$$\lambda_D = \sqrt{\frac{\varepsilon_0 k_B T_\alpha}{n_\alpha q_\alpha^2}} \tag{3.2}$$

Fluid equations The interaction between components in a plasma happens through electro-magnetic forces, each particle interacting at the same time with any other in the volume. A precise description of the plasma medium is obtained from the kinetic theory. The probability density function $f_\alpha(\underline{\mathrm{x}}, \underline{\mathrm{v}}, t)$ represents the position of the plasma components of specie α in the $6-$dimensional phase space. From the definition of f_α it follows:

$$\begin{cases} n_\alpha(\underline{\mathrm{x}}, t) &= \int f_\alpha(\underline{\mathrm{x}}, \underline{\mathrm{v}}, t)\, \mathrm{d}^3 v \\ \\ \langle\psi\rangle_\alpha(\underline{\mathrm{x}}, t) &= \dfrac{1}{n_\alpha} \int \psi\, f_\alpha(\underline{\mathrm{x}}, \underline{\mathrm{v}}, t)\, \mathrm{d}^3 v \end{cases} \tag{3.3}$$

Each of the functions must verify the Boltzmann equation which states that[13]

$$\frac{\mathrm{d}f}{\mathrm{d}t} = \left(\frac{\partial f}{\partial t}\right)_{(coll)} \tag{3.4}$$

or

$$\frac{\partial f}{\partial t} + \underline{\mathrm{v}} \cdot \frac{\partial f}{\partial \underline{\mathrm{x}}} + \frac{\underline{\mathrm{F}}}{m} \cdot \frac{\partial f}{\partial \underline{\mathrm{v}}} = \left(\frac{\partial f}{\partial t}\right)_{(coll)}. \tag{3.5}$$

Equation (3.4) states that the convective derivative in the phase space doesn't change unless collisions happen. When describing a plasma, the equation (3.5) is changed to the Vlasov equation:

$$\frac{\partial f_\alpha}{\partial t} + \underline{\mathrm{v}} \cdot \frac{\partial f_\alpha}{\partial \underline{\mathrm{x}}} + \frac{q_\alpha}{m_\alpha} (\underline{\mathrm{E}} + \underline{\mathrm{v}} \times \underline{\mathrm{B}}) \cdot \frac{\partial f}{\partial \underline{\mathrm{v}}} = 0 \tag{3.6}$$

In the Vlasov equation the collision term is dropped and the Lorenz terms are expressed in function of the self consistent fields, $\underline{\mathrm{E}}$ and $\underline{\mathrm{B}}$; these fields are generated by the plasma itself and satisfy the Maxwell equation with the source terms

$$\rho = \Sigma_\alpha\, q_\alpha \int f_\alpha \mathrm{d}^3 v \qquad \underline{\mathrm{j}} = \Sigma_\alpha\, q_\alpha \int \underline{\mathrm{v}} f_\alpha \mathrm{d}^3 v \tag{3.7}$$

The set of equations that enable the fluid treatment of the plasma (fluid equations) is obtained by calculating momenta $\psi(\underline{\mathrm{v}})$ of the Vlasov equation at different orders. When calculating the equation for a given order, a term of higher order in $\underline{\mathrm{v}}$ appears, due to the second term in equation (3.6). A hierarchy of equations is hence created, where each equation contains a term that is defined in the one of higher order. This hierarchy can be stopped whenever physical consideration enable the dropping of the highest order term. At the first two orders, respectively for $\psi = 1$ and $\psi = m\underline{\mathrm{v}}$, one obtains[1]:

$$\frac{\partial n_\alpha}{\partial t} + \underline{\nabla} \cdot (n_\alpha \underline{\mathrm{u}}_\alpha) = 0 \tag{3.8}$$

$$m_\alpha n_\alpha \frac{\mathrm{D}}{\mathrm{D}t}\underline{\mathrm{u}}_\alpha = -\underline{\nabla} \cdot \underline{\underline{\mathrm{P}}}_\alpha + q_\alpha n_\alpha \left(\underline{\mathrm{E}} + \underline{\mathrm{u}}_\alpha \times \underline{\mathrm{B}}\right). \tag{3.9}$$

where have been introduced the fluid velocity $\underline{\mathrm{u}}_\alpha = \langle \underline{\mathrm{v}} \rangle_\alpha$ and the pressure tensor $\underline{\underline{\mathrm{P}}}_\alpha = \langle \underline{\mathrm{vv}} \rangle_\alpha$. In the non viscous approximation the pressure tensor $\underline{\underline{\mathrm{P}}}_\alpha$ is diagonal and can be written in the form

$$\underline{\underline{\mathrm{P}}}_\alpha = p_j \underline{\underline{\mathbf{1}}} = n_\alpha T_\alpha \underline{\underline{\mathbf{1}}} \tag{3.10}$$

where T_α is the kinetic temperature for the α component. In the cold plasma approximation, which is used in forthcoming chapters, it is set $T_\alpha = 0$ in (3.10).

3.2 Plasma created by lasers

The interaction between laser pulses, at a flux over a certain threshold, and supercritical matter (i.e. $\omega_{pe} > \omega_{laser}$) produces a plasma. As a general scenario, electrons are heated at first, by the evanescent wave that penetrates the skin depth $l_s = c/\omega_{pe}$, atoms are ionized and a high temperature corona of plasma starts to expand from the area of interaction. The involved mechanisms range depending on the intensity and the duration of the laser pulse.

3.2.1 Matter ionization and plasma creation

When high intensity electromagnetic (em) radiation interacts with matter, electrons start to oscillate accordingly to the forcing electric field. As intensity increases, the field amplitude becomes comparable to the bounding field of the outer electronic shells (or

[1] Defined the convective derivative $\frac{\mathrm{D}}{\mathrm{D}t} = \frac{\partial}{\partial t} + \underline{\mathrm{u}} \cdot \underline{\nabla}$.

electrostatic potential comparable to the work potential) and nonlinear effects gain in importance. [51, 81, 82]. If no resonant level exists, the direct, single photon, ionization is impossible; when the density of photons is sufficiently high, different ionization mechanisms (nonlinear ionizations) can happen; their small cross section makes them not observable at lower intensities. The relative importance of these cross sections has been extensively studied. The adiabaticity parameter (the Keldysh factor)

$$\gamma_K = \frac{\omega}{\omega_t} = \omega \frac{\sqrt{2mW}}{eA} \tag{3.11}$$

is defined as the ratio between the laser frequency ω and the frequency ω_t of electron tunnelling through a potential barrier. This last comes from the ratio between the electron potential in the oscillating field eA and its ionization momentum $\sqrt{2mW}$, set W the work potential of the level. The value of (3.11) defines the main ionization mechanism, as briefly described hereafter in order of increasing field amplitude.

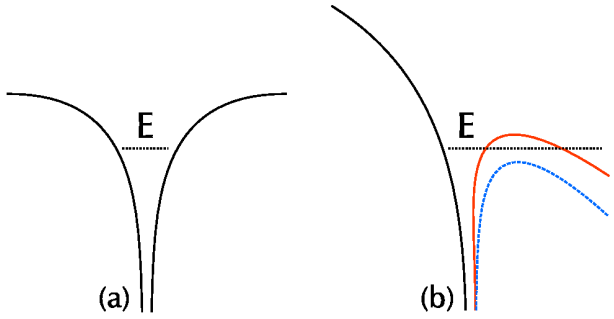

Figure 3.1: Non linear ionization: the electron in the potential well can tunnel through the residual potential (red) of is freed by suppression of the barrier (blue)

Multiphoton ionization For values of $\gamma_K > 1$ the only possible mechanism is the multiphoton ionization. When a sufficient density of photon exists, a bound electron can be freed by the absorption of several photons with an energy lower than the work potential[100, 1, 64]. The typical threshold value ranges between $10^{10} W/cm^2$ and $10^{14} W/cm^2$. In above-threshold ionization (ATI, [2, 34]) more photons are absorbed than necessary for the ionization. In this cases electrons are freed with non-zero energy, and their spectrum shows peaks around multiples on the photon energy, $h\nu$.

Tunnel ionization When $\gamma_K < 1$ the walls of the potential well are deformed in a way that only a finite range of forbidden energies exists for the bound electron. A non-zero probability exists for the electron to tunnel through the potential barrier (Fig.3.1-red).

Suppression of the potential barrier When the well boundary is deformed to have its maximum lower than the energy of the bound electron (Fig.3.1-blue), no more barrier exists and the electron drifts in the electric field ($\gamma_K \ll 1$).

3.2.2 Correlation with the pulse duration

ns pulses

When a *nanosecond* laser pulse interacts with matter, atoms are ionized by multiphoton ionization and electrons accelerated in the laser electric field. In metals the temperature of electrons in conduction band is strongly increased and new electrons from inner shells are promoted to it. In transparent dielectrics electrons have to be freed before any absorption could take place, and this motivates the higher threshold of damage.

In both cases the plasma is produced by collisions between the quivering electrons and the matter at rest. The threshold fluxes for $\tau_L = 1ns$ are of the order of $I\tau_L \gtrsim 1.5J/cm^2$ for gold and $I\tau_L \gtrsim 40J/cm^2$ for fused silica (Fig.3.2). In the ns regime, the laser dura-

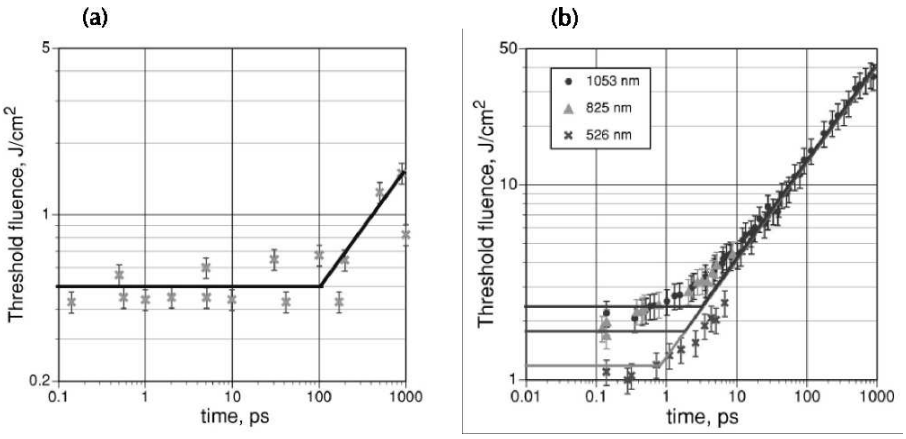

Figure 3.2: Damage thresholds at different pulse length for gold (a) and fused silica (b). (Ref.[30])

tion is longer than the characteristic timescale of thermal processes, which brings to the

quasi-stationary formation of three areas, namely a **corona**, a **conduction region** and a **shocked region**. In the corona ($n_e < n_c$) the laser energy is absorbed by electrons in the plasma at undercritical density[2]; in the conduction region ($n_c < n_e < n_s$) the thermal conduction transports energy from the laser-heated region to the bulk; in the shocked region ($\rho > \rho_s$) the matter is compressed to densities higher than the solid (ρ_s) by conservation of momentum from the expanding motion in the corona (rocket effect). This last effect is responsible for the creation of a shock wave, which propagates towards the unperturbed part of the bulk. During the laser pulse duration, the expansion of the corona in the vacuum can be regarded as isothermal.

sub-*ps* pulses

When the laser duration is $\tau_L < 1ps$, the interaction process with cold matter changes due to (i) the short duration and (ii) the higher intensities reached.
The laser pulse duration is shorter than the characteristic times of electron-to-ion energy transfer, the electron heat conduction and the time of hydrodynamic expansion of the interaction zone. This makes the laser pulse to interact with a solid target where the density remains almost constant.

The higher intensities ($I \sim 10^{13} - 10^{14}\, W/cm^2$ at the threshold) are responsible for almost sudden ionization at the beginning of the laser pulse, not depending on the nature of the material, metal or dielectric. Ablation of the material can happen for charge separation in the interaction zone. Electrons can gain sufficient energy to escape the target and drag ions out of it (when $\varepsilon_e > \varepsilon_{work} + \varepsilon_b$)[3] or can be pushed deeper by ponderomotive force. The expansion starts once the laser pulse has passed over and it can be regarded as adiabatic, where a plasma front propagates towards the vacuum at a speed of

$$v_p = \frac{2\gamma_A^{1/2}}{\gamma_A - 1} c_{s\,0} \tag{3.12}$$

and the transition between the unperturbed bulk and the shocked region at

$$v_s = -\gamma_A^{1/2} c_{s\,0} \tag{3.13}$$

[2]Defined n_c the electron density for which $\omega_{laser} = \omega_{pe}$.
[3]Where are defined ε_e the electron energy, ε_{work} the electron work potential and ε_b the ion work potential.

having defined

$$c_{s0} = \sqrt{\frac{(Z+1)\,k_B T_i}{A m_i}} \tag{3.14}$$

the isothermal speed of sound in the unperturbed material and $\gamma = 5/3$ the adiabatic constant[22].

3.3 Electron Heating from UHI lasers and particle acceleration

This thesis falls in the context of the interaction between Ultra High Intensity (UHI) femtosecond lasers and supercritical matter. At relativistic intensities ($I_0 > 10^{18}\,W/cm^2$) from CPA laser chains (Ch.2) the interaction with a ns pedestal at intensities over the ionization threshold, is to be accounted for before the sub-ps peak. The considered situation is then an UHI, sub-ps pulse interacting with a preformed expanding plasma. In this section I focus on the mechanisms of energy transfer between the laser pulse and the existing plasma gradient, which are responsible for the generation of a suprathermal electron population.

When the *em* wave penetrates the plasma gradient, it propagates freely until the critical surface at density

$$n_c = \frac{\varepsilon_0 m_e}{e^2}\omega \tag{3.15}$$

which is obtained by equating $\omega = \omega_{pe}$ from (3.1). If the field amplitude is relativistic, the electron plasma frequency is corrected by the increase of the accelerated electrons' mass (induced transparency), giving

$$\omega'_{pe} = \sqrt{\frac{1}{\gamma}}\,\omega_{pe} \tag{3.16}$$

The free electrons are made slowly drifting by the $v \times B$ term in the Lorenz force while oscillating in the electric field. The only way to make them gain a net energy from the interaction is to break the adiabaticity of the process, i.e. make them escape the interaction region once they have gained momentum. In a plasma this can happen due to collisionality, wave breaking or steep discontinuities in the density distribution.

Collisional absorption (inverse Bremsstrahlung)

When an electron in its quivering motion in the laser field ω undergoes a collision with an ion, its trajectory in the electric field is lost and a local conversion to thermal energy happens. Given ν_{ei} the electron-ion collision frequency, the overall effect is accounted for an absorption rate of[35, 101, 86]:

$$A_{coll} = \frac{\omega}{\omega_{pe}} \left(\frac{8\nu_{ei}}{\omega} \right)^{1/2} \tag{3.17}$$

where ω_{pe} is the usual electron plasma frequency. From the Spitzer collision frequency for hot plasma[14, 94]

$$\nu_{Spitzer} \;=\; \frac{4}{3}\sqrt{2\pi}\, \frac{Z^* e^4}{16\pi^2 \varepsilon_0^2}\, \frac{m_e n_e}{(m_e k_B T_e)^{3/2}} \ln\left(\Lambda'\right) \tag{3.18}$$

the collisionality decreases as temperature increases (for the definition of Λ' see (5.4)). This mechanism is most effective at lower laser intensities: in the high intensity limit, the thermal motion of electrons becomes much smaller than their velocity in the laser field. The collisional absorption is considered to be negligible for laser intensities higher than $10^{16} W/cm^2$.

ponderomotive forces and $j \times B$ heating

In presence of an electro-magnetic field, a charged particle is subject to the usual Lorentz force.

$$\underline{\mathrm{F}}_L = \frac{q}{m} \left(\underline{\mathrm{E}} + \underline{\mathrm{v}} \times \underline{\mathrm{B}} \right) \tag{3.19}$$

In an electromagnetic wave, the coupling between the E-field and the B-field make the particle to drift in the direction of propagation while quivering in the oscillating electric field. When the field amplitude is not constant in space, a force term, directed along the intensity gradient appears[76, 75]. In the classical limit[54], the oscillation center of a free charge q in the *em* field $\underline{\mathrm{E}}$ at frequency ω_0 is governed by the force

$$\underline{\mathrm{F}}_p \;=\; -\underline{\nabla}\Phi_p; \quad \Phi_p \;=\; -\frac{q^2 \left|E_0\right|^2}{2 m_0 \omega_0^2} \cos\left(2\omega_0 t\right). \tag{3.20}$$

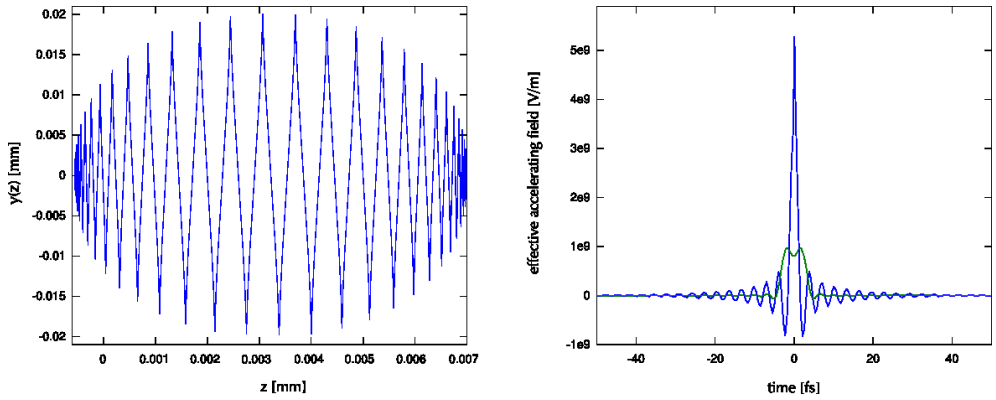

Figure 3.3: Trajectories *(left)* and effective accelerating field due to ponderomotive potential *(right)* for an electron in a short electromagnetic pulse (numerical simulation). The pulse ($\tau_L = 30fs$, $I_0 = 10^{15} W/cm^2$) propagates along $-\hat{z}$ and is polarized on $\hat{y}$. The green plot represents the averaged force term.

The time averaged value of (3.20)

$$\langle \underline{\mathrm{F}}_p \rangle = -\frac{q^2}{4m_0\omega_0^2} \underline{\nabla}|\underline{\mathrm{E}}|^2 \tag{3.21}$$

represents a net force which pushes the charges, independently of their sign, out of the influence of the higher intensity *em* field; being dependent on the $mass^{-1}$, its effect is predominant on the electron component. The ponderomotive push is responsible of the *hole boring* in the target surface[84] and the steepening of the plasma density gradient[25, 6].

The oscillating term at $2\omega_0$ in (3.20) is responsible for the so-called $j \times B$ heating[53]. The non-adiabaticity of electrons in the skin depth, while oscillating in the non-resonant $2\omega_0$ term, can be broken. This happens while following a trajectory which pushes them into the overdense plasma, making them to escape the region of influence of the oscillating force[101].

Resonant absorption and Wavebreaking

It is considered the propagation of a p-polarized wave with vector $\underline{\mathrm{k}} \equiv (k_x, k_y)$ through a plasma density gradient $\underline{\nabla} n_e \parallel \hat{x}$. The local permittivity in the plasma is written as

$$\frac{\varepsilon(x)}{\varepsilon_0} \approx 1 - \frac{\omega_{pe}^2(x)}{\omega_0^2}\left(1 + \frac{\mathrm{i}\nu}{\omega_0}\right) \tag{3.22}$$

where ν is the collision frequency. In the collisionless limit the ratio $\nu/\omega_0 \to 0$, which produces a singularity at the critical surface, where ω equals ω_{pe}. In [27] the numerical solutions of the light propagation equations are presented. At the critical boundary the only non-zero magnetic component (B_z) is purely real, with $B_z > 0$ for $n_e < n_c$ and $B_z = 0$ otherwise. The electric field E_x stays real and is proportional to $1/\nu$, which makes it to diverge in the collisionless limit. From the Ampere's equation on x, $\partial_y B_z = \mu_0 J_x + \partial_t E_x$ a strong electron current arises. The physical situation is the one on an electron plasma wave that is resonantly driven by the forcing field. The electron current in x absorbs energy from the laser wave and the amplitude of oscillations grows in time. The resonant absorption is present only for p-polarized waves, as the electric field component that is normal to the critical surface is needed to drive the plasma oscillations across it. Moreover, the effect is set up only when the plasma gradient length is bigger than the laser wavelength, $L_{grad} \gg \lambda$. An estimate of the ratio of energy absorption is [101]

$$A_{resonant} \approx \frac{1}{2}\left[2.3\,(k_0 L_{grad})^{1/3}\sin(\theta)\cdot\exp\left(-\frac{2}{3}k_0 L_{grad}\sin^3(\theta)\right)\right] \tag{3.23}$$

which shows a maximum for $\theta \approx \arcsin(1/k_0 L_{grad})^{1/3}$. The resonant absorption is the main electron heating process for fluxes $10^{12} W\cdot\mu m^2/cm^2 < I\lambda_{\mu m}^2 < 10^{17} W\cdot\mu m^2/cm^2$.

Wavebreaking As the previously described effect evolves in time, the plasma waves that set up in outer regions, $n_e < n_c$, start to de-phase from the driver, as their self oscillating frequency is different from the forcing one, while the resonant wave grows in amplitude. This produces a shrinking of the resonance area. The waves break when the fluid elements from two regions with a different relative phase come to cross each other's trajectories. In particular if a phase difference of $\pi/2$ exists between the outer and the inner oscillation, some electrons are injected in an inner wave, finding a strong accelerating field, leaving the influence of the driver and propagating in direction of higher densities[27, 3].

vacuum heating (Brunel effect)

When a strong oscillating electric field acts orthogonally on the separation between a conductor and vacuum, electrons can be pulled out of the conductor and sent back at a velocity comparable to their oscillating velocity in the quivering motion,

$$\beta_{osc} = \sqrt{\frac{a_\perp^2}{a_\perp^2 + 1}}. \tag{3.24}$$

The vacuum heating is found to be more important than the resonant absorption when the gradient length L at the critical surface becomes smaller or comparable to the electron displacement in the $\hat{z} = \underline{\nabla} n_e$ direction. An estimation of laser energy absorption is [11]:

$$A_{brunel} = \frac{\eta}{\pi} \frac{a_\perp}{a_0^2 \cos(\theta)} \left[\sqrt{(1 + a_\perp^2)} - 1 \right] \tag{3.25}$$

where the terms a_0 and $a_\perp$ are respectively the dimensionless amplitude for the total electric field and its component on $\hat{z}$. The factor η is calculated numerically [11] and found to be, in the relativistic case, $\eta = 1.66$ for $a_\perp = 2$. This effect is active only for p-polarized light.

3.4 Laser ion acceleration

Two separate mechanisms of laser ion acceleration are at present recognised and confirmed by experiments and PIC simulations: front surface and rear surface acceleration. This last is normally termed TNSA (Target Normal Sheath Acceleration). In this theoretical introduction as well as in proton acceleration experiments, I only focused on protons which acquire a final velocity in the forward direction. A proton beam emerging from the illuminated surface and propagating backwards is found in PIC simulations and experimentally observed by some experimental teams, as a consequence of the plasma expansion from that surface. When using a high contrast laser on very thin targets [12], the backward acceleration conditions are the same as the forward ones, which makes the two spectra and cutoffs comparable.

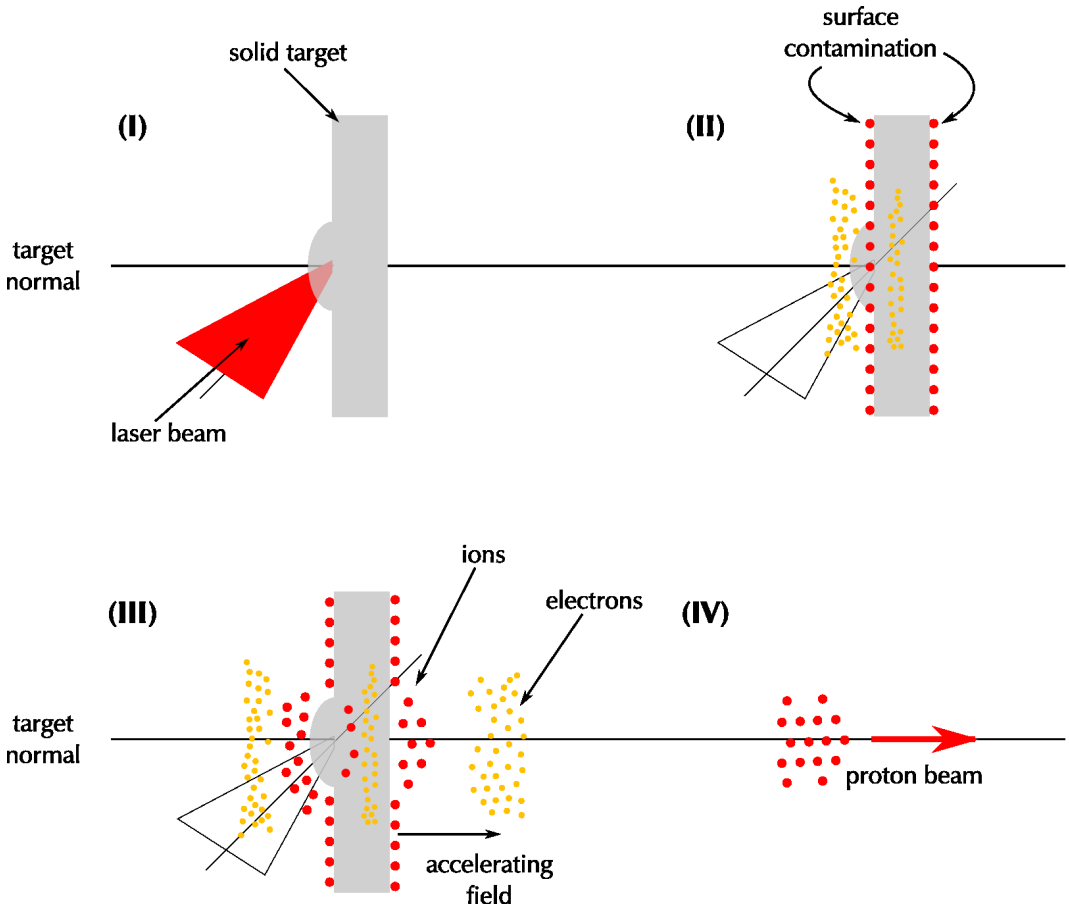

Figure 3.4: Proton acceleration scheme. The UHI laser pulse impinges on a slab of solid matter (I); the matter is ionized and the plasma heated, which produces suprathermal electron population (II). Following the propagation of electrons through the target (III) an electrostatic accelerating field is set up on the rear surface (TNSA), which extracts and accelerates ions from the back surface impurities.

3.4.1 Acceleration from the illuminated surface

Ions are accelerated at the front (illuminated) surface by the charge separation that is induced in the expanding plasma. Depending on the mechanism that dominates in the electron heating, the correlation with laser parameters changes. In cases of normal incidence or s-polarized obliquely incident light, the main charge separation mechanism at relativistic intensities is due to the ponderomotive potential, thus the acceleration gradient lies on the axis of laser propagation [83]; as a consequence of the radial components of the ponderomotive force, a non negligible charge separation on the target

normal direction can be however set up. From [83] the scaling of the cutoff energy for protons from the front surface and normal incidence of the laser is

$$E_{MAX}^{(front)} \approx 2\sqrt{2}aZ \times 0.511MeV, \tag{3.26}$$

where a is the renormalized field amplitude (2.14).

For p-polarized light, independently from the scale gradient length [40], the heating mechanisms, resonant and vacuum heating, are directed along the normal, and so the accelerated ion beam. From [39] the front ion acceleration can be seen as a balance between the thermal pressure and the laser pressure:

$$\frac{\mathrm{d}E_i}{\mathrm{d}t} = (1+R)\frac{I_0}{cl_s} - \frac{n_e k_B T_e}{L_{grad}} \tag{3.27}$$

3.4.2 Rear surface acceleration

When a hot plasma is not confined, its internal pressure leads to its expansion. We observe the formation of a density gradient, density being lower at peripheral regions, and the propagation of a rarefaction wave towards the higher densities. The local charge neutrality holds up to its local Debye length (3.2). The difference in mass between electrons and ions produces a separation of charges at the plasma/vacuum interface; the suprathermal part of the electron spectrum enhances this separation, which results in an accelerating field that drags and accelerate the initially cold ions[38, 98].
The suprathermal electron population that is produced in the laser-plasma interaction drifts through the target. Upon its arrival onto the rear surface, the matter is ionized by resistive heating and collisions; the resistive heating happens as a consequence of the ultra strong currents that re-equilibrate the charge unbalance. The divergence of the electron flux travelling through the bulk is in some part considered responsible of the decrease of ion energy that is observed on thicker targets. In [89] the divergence is measured by looking at the *Optical Transition Radiation* (OTR) emission on the rear surface of targets of different thicknesses. The measured half width at half maximum (HWHM) corresponds to an angle of 17°[4]. More recent experiments [90] repeated the

[4]The experiment was held in the *Laboratoire pour l'Utilisation des Lasers Intenses* (LULI) of the École Polytechnique and the focusing parabola had $f/3$ aperture.

measure by observing the *Coherent Transition Radiation* (CTR) emission. They underlined a double structured transport, with a hotter and narrower bunch ($\approx 10MeV$ at $\sim 7°$ HWHM), followed by a colder and more divergent ($\approx 600keV$ at $\sim 35°$ HWHM). The second one contains the larger part (some tens of percent) of the total laser energy.

In the following sections, two analytical models for TNSA ion acceleration are presented.

Isothermal Model In [74] and in later improvement [71] is presented the solution for the expansion of an isothermal plasma where $T_e \neq T_i$. At $t = 0$, a semi-infinite plasma occupies the $(-\infty, 0]$ space; ions are cold whereas an electronic temperature T_e exists. No cold electrons are taken in account and the neutrality is written as $n_{e\,0} = Zn_{i\,0}$. The electron population respects the Boltzmann distribution

$$n_e \;=\; n_{e\,0}\, \mathrm{e}^{e\Phi/k_B T_e} \tag{3.28}$$

under the action of the electrostatic potential Φ

$$\varepsilon_0 \frac{\partial^2 \Phi}{\partial x^2} \;=\; e\,(n_e - Zn_i) \tag{3.29}$$

The electric field at $x = 0$ is obtained by integration of (3.29), which produces [16]

$$E_{front,0} \;=\; \sqrt{\frac{2}{e}} \cdot \frac{k_B T_e}{e\lambda_{D\,0}} \tag{3.30}$$

During the evolution in time the electron component is supposed in equilibrium with the potential, while the ion component is governed by the two fluid equations (3.8) and (3.9) where the force on the electron component derives from the potential Φ:

$$\frac{\partial u_i}{\partial t} + u_i \frac{\partial u_i}{\partial x} \;=\; \frac{Ze}{m_i} \frac{\partial \Phi}{\partial x} \tag{3.31}$$

The set of differential equation (3.8) and (3.31) with the conditions (3.28) and (3.29) has been resolved numerically with a lagrangian code in [74]. The formation of three non-neutral areas is observed (Fig.3.5). Firstly a rarefaction front with positive charge propagates at a speed $-c_s$ in the unperturbed plasma. Secondly a separation of charges forms at the expanding front: an electron cloud followed by an ion front. By fitting the

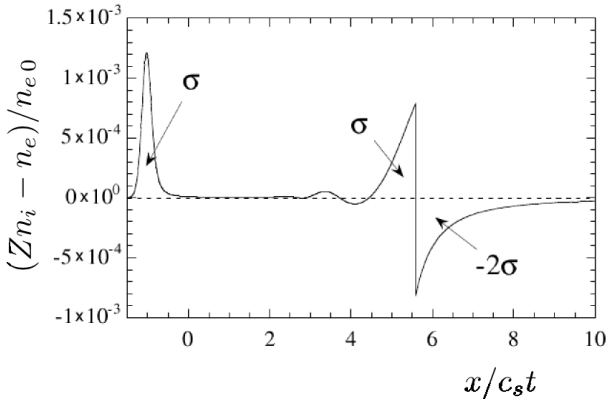

Figure 3.5: The creation of three non-neutral areas during the expansion of the hot electrons, cold ions plasma (excerpt from [71]).

numerical result for the accelerating field at the charge separation front, it is obtained:

$$E_{front} = \frac{2E_0}{\sqrt{2e + (\omega_{pi}t)^2}} \tag{3.32}$$

from which the speed of the ion front is

$$\begin{cases} v_{f,I} &= 2c_s \log\left[\tau + \sqrt{\tau^2 + 1}\right] \\ \\ \tau &= \dfrac{1}{\sqrt{2e}}\,\omega_{pi}t \end{cases} \tag{3.33}$$

where $\omega_{pi} = \left(Zn_{e\,0}e^2/m_i\varepsilon_0\right)^{1/2}$. It has to be underlined that in this calculation the charge neutrality $n_i = n_{e\,0}/Z$ is fixed at the beginning of the simulation, which makes the quantity ω_{pi} dependent on the initial $n_{e\,0}$. The ion energy is finally calculated from (3.33) to be

$$E_{max} = \frac{1}{2}Zk_BT_e\left[2\log\left(\omega_{pi}t\right) - \log\left(2\right) - 1\right]^2 \tag{3.34}$$

In the isothermal model, no energy depletion of the electron component is taken in account. The ions will indefinitely gain energy in time. Rough estimation of a meaningful "acceleration time" correlates with the duration of the laser pulse.

Adiabatic Model The experimental situation of a laser-plasma acceleration on a thin target, differs from the assumption of isothermal model by the fact that *(i)* the finite size of the target doesn't provide an infinite *reservoir* of hot electrons and *(ii)* no external source of energy exists for an indefinite acceleration time.

In [72], an improvement to the isothermal model is presented. At the initial time $t = 0$, the plasma at density ($n_{i\,0}$, $n_{e\,0} = Zn_{i\,0}$) occupies the space $x \in [-L/2, L/2]$ (Fig.3.6). The depletion in energy of the electron component is inserted in the calculation by

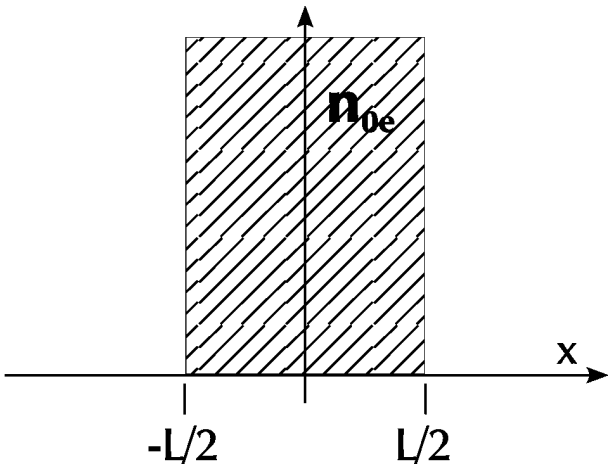

Figure 3.6: Initial condition for the adiabatic model.

$$\frac{\mathrm{d}U_{elec}}{\mathrm{d}t} = -\frac{\mathrm{d}U_{ions}}{\mathrm{d}t} - \frac{\mathrm{d}U_{field}}{\mathrm{d}t}. \tag{3.35}$$

The expansion is symmetric in the two directions, which adds the condition $E\,(x = 0) = 0$ and $v_e\,(x = 0) = 0$ for every time. The system of equations from the isothermal model (3.8), (3.31), (3.28), (3.29) is resolved by the same lagrangian code with the added condition (3.35). In these condition, the solution doesn't change from the isothermal model when $t < t_L$, defined

$$t_L = L/2c_{s\,0} \tag{3.36}$$

the time needed to the rarefaction wave to reach the $x = 0$ boundary.
The simulations show that for $t \ll t_L$ the electron temperature is constant, but that as t approaches t_L the temperature starts falling (Fig.3.7).

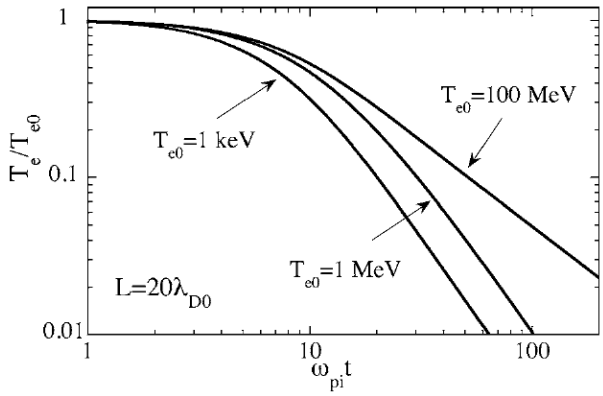

Figure 3.7: Electron temperature decreasing in the adiabatic expansion from a finite size plasma (excerpt from [72]). For an Aluminum target heated at $I = 4 \times 10^{19} W/cm^2$, $T_e \approx 1MeV$ which corresponds to $20\lambda_D \approx 0.4\mu m$. On the time scale, $\omega_{pi} \approx 40ps^{-1}$

The final ion velocity is found to be

$$v_{f,A} \;=\; 2c_{s\,0}\,\log\left[\alpha\frac{L}{\lambda_{D\,0}}+\beta\right] \tag{3.37}$$

where α and β are found to depend on the electron temperature. For $T_e = 1MeV$ it is found $\alpha = 0.49$, $\beta = 5.3$. If we compare (3.37) to (3.33), the two asymptotic behaviours are found to be similar when $L \gg \lambda_{D\,0}$ with an acceleration time of t_L (3.36).

The applicability of each of the two models to the real experimental case of a thin metal foil heated by a laser is bound to the relationship between the two parameters t_l, the laser duration, and $t_e = 2L/c$, the time needed to relativistic electrons to fill the entire thickness[5]. When $t_L \ll t_e$ the interaction between the electron burst and the non-irradiated surface happens only once, which can be considered as the case of an isothermal expansion limited to the duration of the laser pulse, $t_{acc} = t_l$. For $t_e \simeq t_l$, the hot electrons fill the target, making the adiabatic model applicable.

Corrections to the model for finite plasma scale length on the rear surface
In the experimental realization of the plasma slab by means of laser-target interaction, a density gradient on the rear (not illuminated) surface can be produced by the breakout

[5]It holds $t_e[fs] = 6.7\,L[\mu m]$

of the shock wave (see Ch.7). In [73] a correction to the model is presented, which analyses the expansion of a plasma slab when the ion-vacuum front is not steep anymore. A density gradient is introduced at $t = 0$ on the ion front, with a scale length of l_{ss}

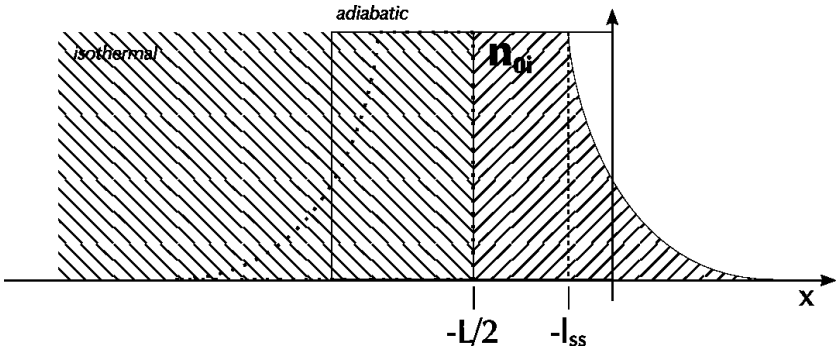

Figure 3.8: Picture of the initial condition for the two cases. In the isothermal case, the density is constant $n_i(x, t = 0)$ for $x \in (-\infty, -l_{ss}]$ and exponentially decreases on the right hand side of $x = -l_{ss}$. In the adiabatic case, the plasma initially occupies the $x \in [-L, 0]$; the symmetry axis is set at $x = -L/2$ and the two density gradients begin at $x = -l_{ss}$ and $x = l_{ss} - L$.

(Fig.3.8). The evolution of the system is analyzed for both the models (isothermal and adiabatic). According to the different representations of the initial system, the corrections are introduced as follow.

Isothermal The cold ion density distribution is

$$\begin{cases} n_i\,(x, t = 0) &= n_{i\,0} & x \le -l_{ss} \\ \\ n_i\,(x, t = 0) &= n_{i\,0} \cdot \mathrm{e}^{-\frac{x+l_{ss}}{l_{ss}}} & x > -l_{ss}. \end{cases} \tag{3.38}$$

The density gradient starts at $x = -l_{ss}$ and the constant density plasma sits in the half-space for $x < -l_{ss}$.

Adiabatic The situation depicted in Fig.3.6 is modified in a way that the new symmetry axis is $x = -L/2$ which make the plasma slab to be initially between $-L$ and 0 for $l_{ss} \to 0$. The gradient envelope is the same as defined in (3.38) for $x > -L/2$ and is symmetrized accordingly for the left hand side.

Aside of this, the physical scenario is the same as previously described, i.e. the ions are initially cold and the electron temperature is set to $T_{e\,0}$. As the system is let

evolve, by solving the set of fluid equations, the ions in the more peripheral region are accelerated by a charge separation field that is weaker than what experienced by those in the denser plasma. The differential gain in energy brings to the crossing between the two populations: the more internal and faster ions overrun the external and slower and the plasma fluid comes to a wave breaking.

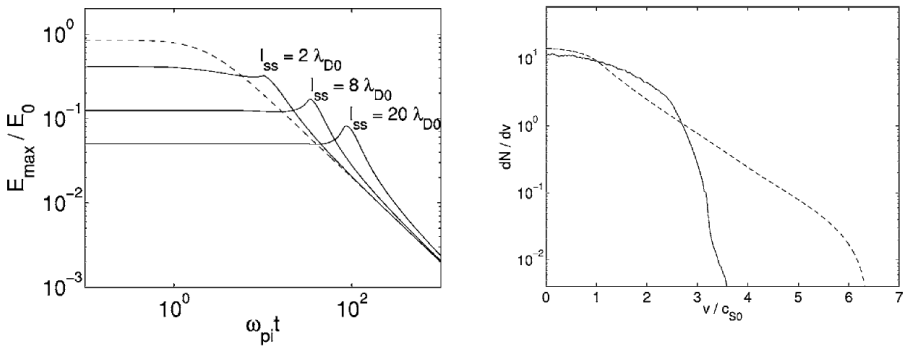

Figure 3.9: *(left)* The evolution in time of the accelerating field due to charge separation at the plasma boundary for different initial density gradient lengths. The dashed line represents the ideal ($l_{ss} = 0$) case for comparison; the peaks in the plot mark the moment when the breaking of the wave happens. *(right)* Final ion velocity spectrum for a sharp boundary (dashed) and $l_{ss} = 20\lambda_{D\,0}$ (solid) from an adiabatic simulation of $L = 40\lambda_{D\,0}$. (Excerpts from [73]).

The evolution in time of the accelerating field for fast ions is shown in Fig.3.9-*left* for different initial conditions. After an initial, constant, accelerating field, a peak appears at the moment the wave breaks; the asymptotic behaviour is found to be the same in all the cases. The accelerating field before the wave breaks is lower for longer plasma scale lengths. A simulation on the adiabatic case, see Fig.3.9-*right*, clearly shows that the final energy that is acquired from a steep boundary plasma is lower than what is achieved in presence of a gradient. Moreover, the longer the gradient, the lower the final ion velocity.